Drag on random assemblies of spheres in shear-thinning and thixotropic liquids

J. J. Derksen[a)]
Department of Chemical and Materials Engineering, University of Alberta, Edmonton, Alberta T6G 2G6, Canada

(Received 28 April 2009; accepted 15 July 2009; published online 5 August 2009)

The flow and resulting drag force in suspensions consisting of monodisperse, solid spheres, and non-Newtonian liquids have been studied via direct numerical simulations. The liquids are purely viscous (i.e., nonelastic) with shear thinning and/or thixotropic (time-dependent) behavior. The configuration of spheres is static. The interstitial liquid flow is solved by means of the lattice-Boltzmann method. Only creeping flow conditions have been considered. Thixotropy enters via a network integrity parameter that relates to the local, apparent viscosity and for which a transport equation has been solved. The results show that the shear-thinning character of the liquid manifests itself more pronounced at higher solids volume fractions. Thixotropy tends to increase the drag force due to the decoupling of locations of high deformation rates and low viscosity. © *2009 American Institute of Physics*. [DOI: 10.1063/1.3200946]

I. INTRODUCTION

Dense solid-liquid suspensions involving non-Newtonian carrier fluids are of practical relevance in applications such as oil sands mining,[1] drilling of oil and gas wells,[2] and food and pharmaceutical processing.[3] Fundamental insights in the interactions of solid and liquid at the level of the solid particles could be relevant for a better understanding of the processes underlying these applications, and thus could help in process design and optimization. Also, process modeling (partly) based on computational fluid dynamics (CFD) at the macroscale has become a viable and widely used approach. Multiphase CFD, however, requires closure relations for mesoscale phenomena such as the hydrodynamic interaction between the phases involved.[4] A lot of research effort has been invested in developing and assessing closures for multiphase systems with a Newtonian carrier phase, such as drag force relations for random particle assemblies,[5,6] and models for turbulent and granular fluctuations.[7] In situations where the carrier phase behaves as a non-Newtonian liquid, the mesoscale fluid mechanics (hydrodynamic interactions, dispersed phase behavior) potentially becomes more complicated. This may have significant implications for the applicability of closures (based on Newtonian fluid concepts) for the mesoscale phenomena of suspensions with non-Newtonian liquids.

With the above in mind we have carried out computational research that aims at assessing non-Newtonian effects in dense solid-liquid suspensions, with a focus on the drag force and the way it depends on liquid properties and the solids volume fraction. The study is limited to suspensions consisting of monodisperse spheres in a purely viscous (i.e., nonelastic) carrier liquid. The sphere assemblies considered are random and homogeneous; there are no large-scale (solids volume fraction) gradients. The liquid flow through the sphere assemblies is slow, i.e., dominated by viscous forces rather than inertia forces.

The type of non-Newtonian liquid model adopted in this study is instigated by the main application of our research which is on oil sands processing, more specifically the handling of its waste streams (tailings, see e.g., Ref. 1). Tailings consist of water, clay particles ("small," surface active solid particles), coarser sand particles, and residual bitumen. The clay particles are the source of non-Newtonian behavior; they tend to form networks, thereby enhancing the consistency of the mixture. The level of integrity of the networks depends on the local flow conditions: Liquid deformation breaks down the network thereby reducing the (apparent) viscosity and thus giving rise to shear-thinning behavior. In addition, clay suspensions have time-dependent rheology. Due to ionic transport limitations at the microscale, the network needs time to build up. Also the breakdown as a result of deformation is not instantaneous. Since the local apparent viscosity depends on the level of network integrity, the deformation history in the liquid influences its rheological behavior which is usually termed thixotropy. Note the multiscale character of the tailings transport behavior and the way this study fits in. The clay particles and their interactions are not explicitly resolved in this study; they are lumped in a non-Newtonian liquid model for the carrier fluid. The present focus is on how the non-Newtonian clay suspension interacts with coarser, solid particles (i.e., sand) that we explicitly resolve. In research on the macroscopic flow behavior of tailings in, e.g., pipeline systems the results of the present study could be used as closures for the interphase (sand-liquid) momentum transfer.

The aim of the paper is to reveal in what way, and to what extent the shear-thinning and time-dependent rheology of the continuous phase influences the drag force on static, random sphere assemblies. The study is purely computational. The flow of interstitial liquid is directly solved by means of the lattice-Boltzmann method (LBM). The trans-

[a)]Electronic mail: jos@ualberta.ca.

port equation describing network integrity is solved in conjunction with the liquid flow with a finite volume scheme. Flow and scalar transport are directly coupled via a relation between local apparent viscosity and network integrity.

The paper is organized in the following manner: First the rheology model is introduced. Then the simulation procedure is outlined. Subsequently verifications regarding system size and spatial resolution are presented. To relate to earlier work from literature, these verifications consider Newtonian liquids. Then we present results regarding the flow of shear-thinning, time-independent (nonthixotropic) liquids through sphere assemblies. The results regarding the drag force are interpreted in terms of the mesoscale flow structures. Finally we consider the effect of thixotropy. At the end the main observations are reiterated.

II. THIXOTROPIC RHEOLOGY MODEL

The thixotropy model we have adopted is based on early work due to Storey and Merrill[8] and Moore,[9] more recently applied by Ferroir *et al.*[10] and Mujumdar *et al.*[11] In this purely viscous model we keep track of a scalar λ that varies between 0 and 1 and indicates the integrity of the network ($\lambda=0$: no network; $\lambda=1$: fully developed network). Its transport equation reads

$$\frac{\partial \lambda}{\partial t} + u_i \frac{\partial \lambda}{\partial x_i} = -k_1 \dot{\gamma} \lambda + k_2 (1-\lambda) \tag{1}$$

(summation over repeated indices implied) with u_i the ith component of the fluid velocity vector, and $\dot{\gamma}=\sqrt{2 d_{ij} d_{ij}}$ a generalized deformation rate; $d_{ij}=1/2[(\partial u_j/\partial x_i)+(\partial u_i/\partial x_j)]$ is the rate of strain tensor. The first term on the right hand side of Eq. (1) indicates breakdown of the network due to liquid deformation; the second term is responsible for build-up of the network with a time constant $1/k_2$ associated to it. In the model, the apparent viscosity μ_a is linked to the network integrity according to

$$\mu_a = \mu_\infty (1+\alpha\lambda), \tag{2}$$

with μ_∞ and α as model constants.

In a homogeneous shear field with shear rate $\dot{\gamma}$, the steady-state solution to Eq. (1) reads

$$\lambda_{ss} = \frac{k_2}{k_1 \dot{\gamma} + k_2}. \tag{3}$$

The associated steady-state viscosity is [combine Eqs. (2) and (3)]

$$\mu_{ss} = \mu_\infty \left(1 + \alpha \frac{k_2}{k_1 \dot{\gamma} + k_2} \right). \tag{4}$$

The parameter μ_∞ can thus be interpreted as the infinite-shear viscosity. The zero-shear viscosity is $\mu_0 \equiv \mu_\infty(1+\alpha)$. A typical representation of the steady-state rheology [Eq. (4)] for $\alpha>0$ is given in Fig. 1. As can be seen, it represents a shear-thinning liquid making the transition from the zero-shear viscosity μ_0 to infinite-shear shear viscosity μ_∞ around a characteristic shear rate $\dot{\gamma}_c \equiv k_2/k_1$. With the latter definition, Eq. (4) can also be written as

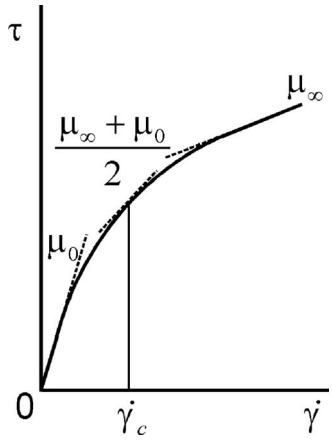

FIG. 1. Steady-state rheology with infinite-shear viscosity μ_∞ and zero-shear viscosity μ_0. At $\dot{\gamma}=\dot{\gamma}_c$, $\mu_{ss}=(\mu_\infty+\mu_0)/2$.

$$\mu_{ss} = \mu_\infty \left(1 + \alpha \frac{\dot{\gamma}_c}{\dot{\gamma} + \dot{\gamma}_c} \right). \tag{5}$$

III. SIMULATION PROCEDURE

A. Flow geometry and boundary conditions

The flow systems we will be considering consist of random solid sphere assemblies with liquid in between. All spheres in the assembly have the same diameter d. The liquid flows through the space not occupied by the spheres with a superficial velocity $\mathbf{u_s}$ as the result of a body force $\mathbf{f}$ acting on the liquid. The body force $\mathbf{f}$ is tuned such that in steady state a preset value of $\mathbf{u_s}$ is achieved. The boundaries of the three-dimensional flow domain are fully periodic. A force balance then implies that that the average drag force $\mathbf{F_D}$ on a sphere in the assembly is[12]

$$\mathbf{F_D} = \mathbf{f} \frac{\pi}{6} d^3 \left(\frac{1}{\phi} - 1 \right), \tag{6}$$

with ϕ as the solids volume fraction of the assembly. This procedure—usually in the context of a lattice-Boltzmann scheme for solving the flow—has been applied by a number of authors to study drag forces due to Newtonian fluid flow as a function of solids volume fraction and/or Reynolds number.[5,6,12–15] More recent simulation studies also involve the effect of suspensions with particles having different slip velocities[16] and particle size distributions.[6] Note that Eq. (6) expresses the convention for the drag force as, e.g., expressed by Van der Hoef *et al.*[6] among others.[14,16,17] The total average force by the fluid on a sphere $\mathbf{F_{f\to s}}$ then is the sum of $\mathbf{F_D}$ and a contribution from the body force (e.g., in its role of an average pressure gradient): $\mathbf{F_{f\to s}}=\mathbf{F_D}+\mathbf{f}(\pi/6)d^3$. It can be verified[6] that $\mathbf{F_{f\to s}}=\mathbf{F_D}/(1-\phi)$.

In Newtonian cases (with dynamic viscosity μ) the drag force [Eq. (6)] is commonly made dimensionless according to $F_D^* \equiv F_D/3\pi\mu d u_s$. Simulations are usually carried out with $\mathbf{f}$ and thus $\mathbf{F_D}$ acting in a specific direction with (as a result) $\mathbf{u_s}$ having the same direction. The scalar values F_D and u_s are the vector components in that direction. Computational re-

sults for monosized spheres and low Reynolds numbers (with $\mathrm{Re}=\rho u_s d/\mu$) have been summarized in correlations in terms of F_D^*, e.g., by Van der Hoef *et al.*,[6]

$$F_D^* = \frac{10\phi}{(1-\phi)^2} + (1-\phi)^2(1+1.5\sqrt{\phi}). \tag{7}$$

The flow of thixotropic liquids (as defined in Sec. II) through monosized sphere assemblies can be pinned down with a set of five dimensionless numbers. In this paper these have been chosen as $\mathrm{Re}_\infty=\rho u_s d/\mu_\infty$, $\mathrm{Db}=u_s/dk_2$, $S=\dot{\gamma}_c d/u_s$, α, and ϕ (Db is the ratio of the time scale of the liquid $1/k_2$ and of the flow d/u_s termed Deborah number; having a Deborah number does not imply viscoelasticity). This five-dimensional parameter space we limit by only considering a single, low value of $\mathrm{Re}_\infty=0.06$. We also fix the viscosity ratio to $\alpha+1=16$. Since $\alpha>0$ the low value of the Reynolds number implies creeping flow conditions at all times.

The particle configurations are created by randomly placing a number of spheres in a cubic domain. Since we are interested in dense suspensions (up to $\phi=0.530$) random placement usually needs to be followed by compacting the particle assembly.[18] After compaction to the desired volume fraction, the configuration is randomized again by giving the spheres random velocities and letting the system evolve for some time as a granular gas with the particles undergoing fully elastic, frictionless collisions. Then the configuration is frozen to be used in the fluid flow simulation procedure.

B. Fluid flow modeling

As in many of the earlier works on the subject of drag on sphere assemblies, we used the lattice-Boltzmann method[19,20] to solve for the flow of interstitial liquid. It has a uniform, cubic grid on which fictitious fluid particle moves in a specific set of directions, and collides to mimic the behavior of an incompressible, viscous fluid. The specific lattice-Boltzmann (LB) scheme employed here is due to Somers.[21] The scheme can accurately account for liquids with nonuniform viscosity as recently demonstrated by Derksen and Prashant.[22] The no-slip condition at the spheres' surfaces was dealt with by means of an immersed boundary (or forcing) method. We have validated and subsequently used this method extensively to study the interaction of solid particles and Newtonian fluids.[17,23–25] For instance, simulation results of a single sphere sedimenting in a closed container were compared to particle image velocimetry experiments of the same system and showed good agreement in terms of the sphere's trajectory, as well as the flow field induced by the motion of the falling sphere.[23]

It should be noted, however, that having a spherical particle on a cubic grid requires a calibration step, as first realized by Ladd.[12] He introduced the concept of a hydrodynamic diameter. The calibration involves placing a sphere with a given diameter d_g in a fully periodic domain in creeping flow and (computationally) measuring its drag force. The hydrodynamic diameter d of that sphere is the diameter for which the measured drag force corresponds to the expression for the drag force on a simple cubic array of spheres due to Sangani and Acrivos,[26] which is a modification of the analytical expression due to Hasimoto.[27] Usually d is slightly bigger than d_g with $d-d_g$ typically equal to one lattice spacing or less. The issue of the hydrodynamic diameter is particularly important in this study since the deviation of d from d_g is a function of the viscosity of the liquid[12,23] and since in this study the liquid's viscosity varies over the sphere's surface with an *a priori* unknown distribution. We have dealt with this issue by assessing the resulting error in the drag force and reducing it to an acceptable level. The relative error in the drag force can be controlled by means of the spatial resolution of the simulations. Since $d-d_g$ typically equals one grid spacing, increasing d relative to the grid spacing reduces the relative deviation $(d-d_g)/d$, and thus the relative deviation in the drag force. In the Sec. IV the quantitative details are discussed.

C. Scalar transport modeling

Having a thixotropic liquid requires solving a transport equation in the network integrity parameter, Eq. (1). This we do by means of a finite volume scheme on the same (uniform and cubic) grid as the lattice-Boltzmann discretization. An advantage of employing a finite volume formulation (over, e.g., also using the LBM for scalar transport modeling) is the availability of methods for suppressing numerical diffusion. This is particularly important in the present application since Eq. (1) does not have a molecular or turbulent diffusion term; in order to correctly solve Eq. (1) we cannot afford to have significant numerical diffusion. As in previous works,[28] total variation diminishing discretization with the Superbee flux limiter for the convective fluxes[29] was employed. We step in time according to an Euler explicit scheme. The deformation $\dot{\gamma}=\sqrt{2d_{ij}d_{ij}}$ and the liquid velocity u_i come from the LBM; the distribution of λ is fed back to the flow solver part by running the LBM with the apparent viscosity field μ_a stemming from Eq. (2). This makes the scalar transport and the LBM part of the simulation procedure two way coupled. The above procedure for performing flow simulations involving thixotropic fluids has been successfully verified by comparing simulation results with semianalytical solutions for a few canonical flows.[22]

At the spherical solid-liquid interfaces the $\partial\lambda/\partial n=0$ boundary condition is imposed via interpolation: Grid points inside the sphere, close to the surface, are given a value of λ equal to the interpolated value of λ, one outward normal unit vector away from that point. These "ghost" values of λ inside the spheres are used as boundary conditions in the explicit update of the λ-transport equation in the liquid volume.[28]

IV. VERIFICATION

As explained above, the issue of the hydrodynamic diameter versus the given diameter and the dependence on the viscosity of the former require careful consideration. Calibrations according to Ladd[12] were performed with a Newtonian fluid at kinematic viscosity $\nu=0.04$ (in lattice units) such that a set of spheres was created with hydrodynamic diameters of $d=12$, 16, 24, and 32 lattice spacings. Spheres were placed in a random assembly in a cubic domain with vertex length

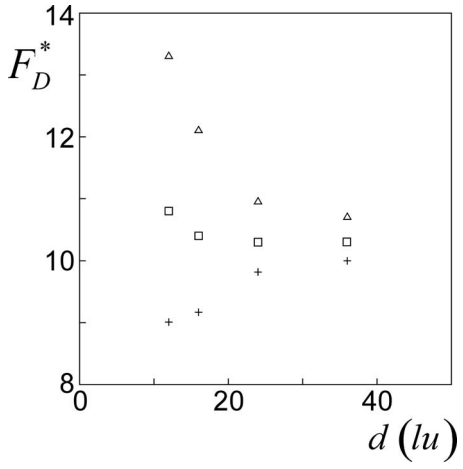

FIG. 2. Dimensionless drag force F_D^* for a Newtonian simulation at Re=0.06 and ϕ=0.373 as a function of the spatial resolution of the simulation expressed in the number of lattice-spacings spanning the diameter d. Squares: ν=0.04 (the viscosity at which d was calibrated); triangles: ν=0.01; plusses: ν=0.16.

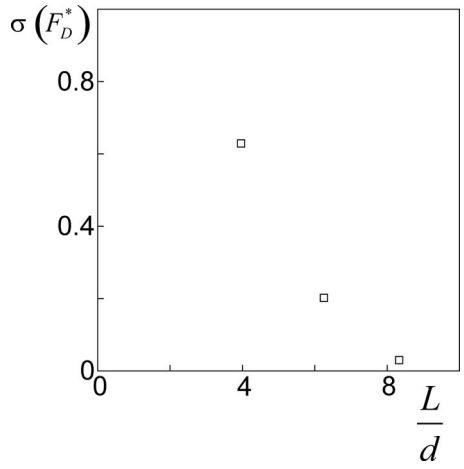

FIG. 3. Standard deviation of F_D^* as a result of variations in the particle configuration as a function of system size L (relative to sphere diameter d). Newtonian simulations with Re=0.06 and ϕ=0.373.

L=6.25d at a solid volume fraction of ϕ=0.373. First a Newtonian liquid with ν=0.04 (i.e., the same viscosity with which the calibrations were done) was forced through this assembly at the four resolutions considered, all four at Re=$u_s d/\nu$=0.06. The results are given in Fig. 2 (square symbols). The relative placement of the spheres is the same in the four simulations; the only difference is the spatial resolution. In terms of F_D^* the results at the three highest resolutions differ less than 5% and can be considered grid independent. Subsequently, we performed simulations with a viscosity being a factor of 4 higher, and a factor of 4 lower than the default viscosity of 0.04 (still Newtonian fluid, still Re=0.06). Now we clearly see the effect of the hydrodynamic diameter being dependent on the viscosity: At the lower viscosity F_D^* gets overpredicted (triangles); at the higher viscosity it gets underpredicted (plusses). As anticipated, however, the deviations are a pronounced function of the resolution. At the highest resolution (d=36) the deviations are typically $\pm$3% at the one but highest resolution (d=24) of $\pm$5%. These deviations are worst-case deviations. In our non-Newtonian simulations the maximum ratio of highest over lowest viscosity is α+1=16, with the center kinematic viscosity $(\mu_\infty+\mu_0)/2\rho$ equal to 0.04. Given the large parameter space and (consequently) large number of simulations to be done, it was decided to perform the remainder of the simulations with a resolution of d=24 and to keep the $\pm$5% error in mind when interpreting the results.

In terms of computational cost, also the size of the flow domain (the ratio of domain size over sphere diameter L/d) is a relevant parameter. Its influence is most strongly felt in terms of statistical fluctuations, i.e., the extent to which the average drag force F_D^* changes from configuration to configuration at constant ϕ. Very large L/d will show minor changes but are computationally expensive, smaller L/d will show stronger case-to-case fluctuations, and at some level will lead to artifacts related to the small system size and periodic boundary conditions. The impact of L/d has been measured in terms of the standard deviation of F_D^* as a function of system size (Fig. 3). At L/d=6.25, $\sigma(F_D^*)/F_D^*$ is less than 0.02, which, given the other uncertainties, is considered acceptable. In the remainder we will stick to L/d=6.25. Furthermore, many of the F_D^* data points presented are the result of averaging over a number (usually 3) of statistically independent sphere configurations.

So far the performance of our simulations procedure has been verified by internal comparisons (comparing simulations done with the same computer code, however, with different numerical and physical settings). Since the immersed boundary method used in this paper[23,30] differs from more common ways to impose no-slip conditions at curved surfaces in the lattice-Boltzmann method (the *de facto* standard being set by Ladd[12]), drag force results have also been compared to results from literature; more specifically the results due to Van der Hoef *et al.*[6] on drag in random, monosized sphere assemblies as a function of the solids volume fraction ϕ at creeping flow conditions and with Newtonian liquids. They summarized their results with the correlation given in Eq. (7). In Fig. 4 that correlation is compared to our simula-

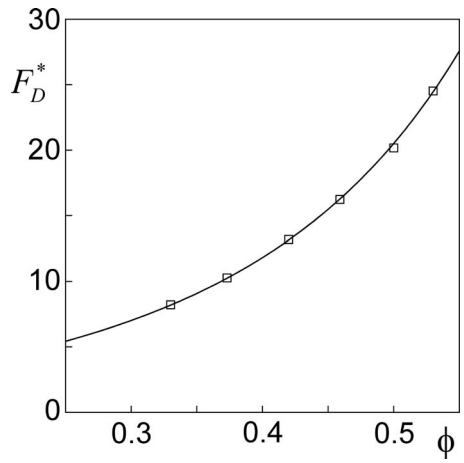

FIG. 4. F_D^* as a function of solids volume fraction ϕ for Newtonian flow at Re=0.06. Solid curve: Eq. (7) [correlation due to Van der Hoef *et al.* (Ref. 6)]; squares: present simulations.

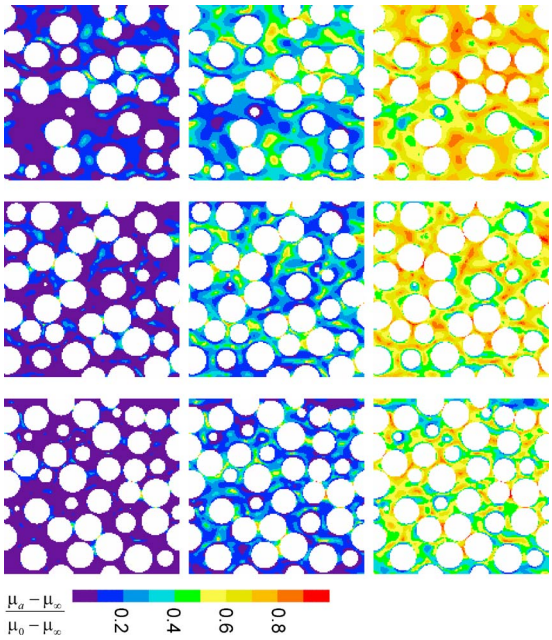

FIG. 5. (Color online) xz-cross sections through the flow domains, with the horizontal (x) direction the direction of the mean flow. Shear-thinning, time-independent liquids. Shades/colors indicate the apparent viscosity. From top to bottom ϕ=0.373, 0.459, and 0.530. From left to right S=1, 4, and 16, respectively.

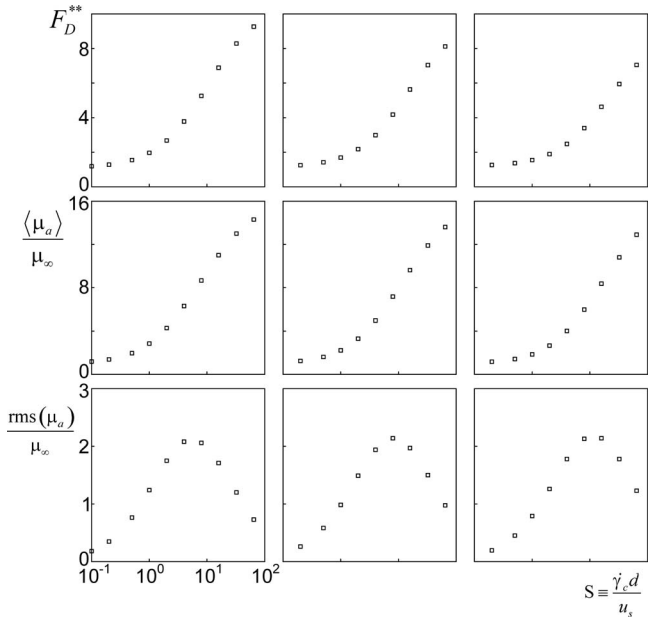

FIG. 6. Doubly normalized drag force F_D^{**} (top), average apparent viscosity $\langle\mu_a\rangle$ (middle), and root-mean-square values of the apparent viscosity $\mathrm{rms}(\mu_a)$ as a function of S for three solids volume fractions: from left to right: ϕ=0.373, 0.459, and 0.530. Shear-thinning, time-independent liquids.

tions at the default settings (Re=0.06, resolution d=24, system size L/d=6.25, ν=0.04, and the hydrodynamic diameter calibrated for this viscosity) showing good agreement. The data points are the average of three sphere configurations. Apparently the resolution is sufficiently high and the Reynolds number sufficiently low to accurately reproduce the empirical correlation [Eq. (7)].

V. RESULTS

A. Shear-thinning, time-independent liquids

Now we turn to drag force results for non-Newtonian liquids. As discussed above, of the five dimensionless numbers governing the flow system, Re_∞ and the viscosity ratio $\alpha+1$ have fixed values, 0.06 and 16, respectively. Initially only shear-thinning, time-independent liquids will be considered. Time-independent liquids have $k_2\to\infty$ so that Db=0. The two degrees of freedom left are the solids volume fraction ϕ and $S=\dot{\gamma}_c d/u_s$. All data points presented in this section of the paper are average values of three statistically independent spherical particle configurations.

In Fig. 5 we show contour plots of the distribution of the apparent viscosity in a cross section through the suspension after steady state has been reached. The cross sections span the xz-plane of the cubic periodic domain with the x-direction the streamwise direction. The white circular disks are cross sections through the spherical particles. The higher the S, the higher the apparent viscosity in the suspension gets. This is not surprising. At higher S (and thus higher $\dot{\gamma}_c$) the transition from zero-shear viscosity to infinite-shear viscosity takes place at higher deformation rates (see Fig. 1). Also the range of viscosities encountered in the suspension is a function of S: If the characteristic shear rate $\dot{\gamma}_c$ of the liquid is of the same order as the shear rates encountered in the interstitial liquid, a relatively broad range of viscosities is anticipated.

The above observations are presented in a more quantitative sense in Fig. 6. The figure shows (for three solids volume fractions) the doubly normalized drag force $F_D^{**}\equiv F_D^*/F_D^*|_{S=0}$. In these non-Newtonian cases F_D^* is based on the infinite-shear viscosity: $F_D^*=F_D/3\pi\mu_\infty d u_s$ and $F_D^*|_{S=0}$ (by definition) is the Newtonian drag force at the specific solids volume fraction normalized with $3\pi\mu_\infty d u_s$. Figure 6 also shows the average apparent viscosity in the suspension, and (as a measure of the spread in viscosities in the liquid domain) the root-mean-square (rms) values of the deviations from the mean apparent viscosity: $\mathrm{rms}(\mu_a)\equiv\sqrt{(1/V_f)\int_{V_f}(\mu_a-\langle\mu_a\rangle)^2 dV}$ with V_f as the volume of (interstitial) fluid. Interestingly $\mathrm{rms}(\mu_a)$ goes through a maximum with the location of the maximum dependent on the solids volume fraction: The higher the ϕ, the further the maximum shifts to higher S. At higher ϕ, the space between the spheres gets narrower and (since the superficial velocity has a fixed value) the deformation rates in the liquid increase. As a result, the distribution of viscosities gets widest for higher $\dot{\gamma}_c$, i.e., higher S.

The increase in the drag force with increasing S as witnessed in Fig. 6 is not solely due to an increase in the average apparent viscosity: If we normalize drag with $\langle\mu_a\rangle$ instead of μ_∞, i.e., define $F_{D,\langle\mu_a\rangle}^*=F_D/3\pi\langle\mu_a\rangle d u_s$ and plot $F_{D,\langle\mu_a\rangle}^{**}=F_{D,\langle\mu_a\rangle}^*/F_D^*|_{S=0}$ the values are significantly lower than 1, see Fig. 7. This is due to the apparent viscosity being lower than the average in high-shear flow regions. The even-

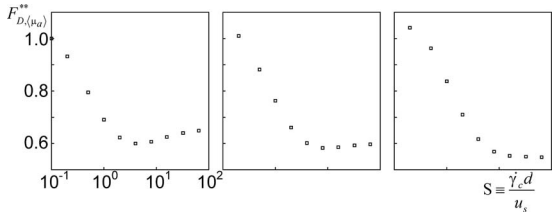

FIG. 7. Normalized drag force $F^{**}_{D,\langle\mu_a\rangle}=F^{*}_{D,\langle\mu_a\rangle}/F^{*}_{D}|_{S=0}$ with $F^{*}_{D,\langle\mu_a\rangle}=F_D/3\pi\langle\mu_a\rangle du_s$ as a function of S for three solids volume fractions—from left to right: ϕ=0.373, 0.459, and 0.530. Shear-thinning, time-independent liquids.

tual drag force is the result of an interplay between the liquid flow through the suspension and the resulting spatial viscosity distribution.

The notion of the interaction between $\dot{\gamma}_c$ and deformation rates in the suspensions has proven helpful in scaling the doubly normalized drag force F^{**}_D. Critical regions in the suspension are the waist-shape gaps between neighboring spheres. As a measure for the typical size of these waists we take $\delta \equiv d[(\phi_{\mathrm{rcp}}/\phi)^{1/3}-1]$ with ϕ_{rcp} as the solids volume fraction at random close packing. For the latter we took $\phi_{\mathrm{rcp}}=0.62$.[31] In Fig. 8 we plot F^{**}_D as a function of $\delta\dot{\gamma}_c/u_s$ for all cases with time-independent rheology (Db=0) considered. The drag force behaves fairly consistently over the wide range of solids volume fractions considered (ϕ from 0.330 to 0.530). Also for the viscosity distribution [as characterized by $\langle\mu_a\rangle$ and rms(μ_a)], the dimensionless group $\delta\dot{\gamma}_c/u_s$ approximately captures the effect of the solids volume fraction, see Fig. 9. The figure also shows that the ratio u_s/δ is a useful deformation rate measure for determining the average viscosity in the suspension.

B. Thixotropic liquids

Finally we investigate the effect of thixotropy (time-dependent rheology) on the liquid flow and resulting drag force in the suspension. The (now three) relevant dimensionless numbers are Db$=u_s/dk_2$, $S=\dot{\gamma}_c d/u_s$, and ϕ. As before

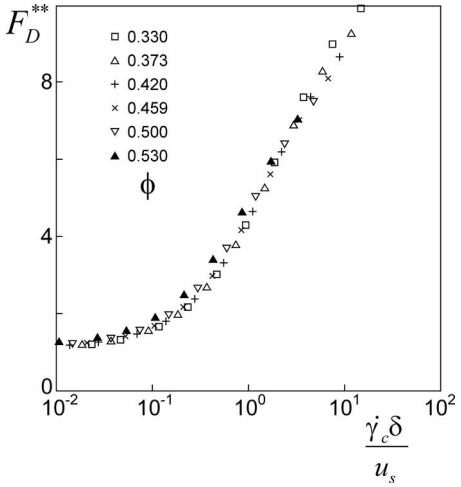

FIG. 8. Doubly averaged drag force as a function of $\dot{\gamma}_c\delta/u_s$ with δ defined in the text. The different symbols relate to different solids volume fraction as indicated. Shear-thinning, time-independent liquids.

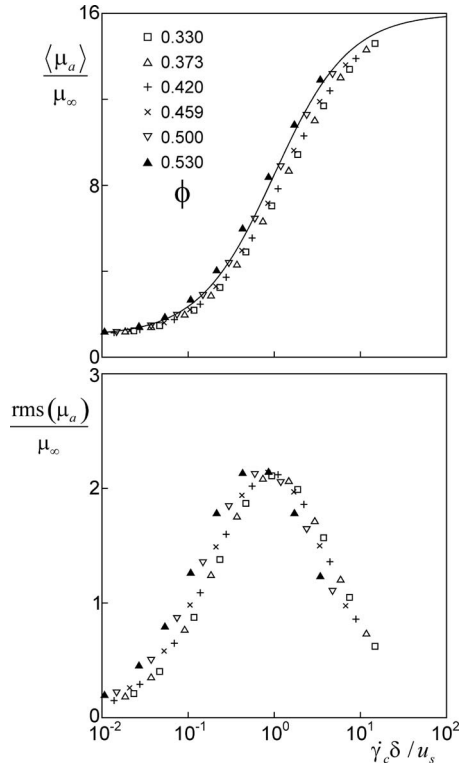

FIG. 9. Average viscosity $\langle\mu_a\rangle$ and rms(μ_a) as a function of $\dot{\gamma}_c\delta/u_s$. The different symbols relate to different solids volume fractions as indicated. The curve on the top panel represents Eq. (5) with $\dot{\gamma}=u_s/\delta$. Shear-thinning, time-independent liquids.

we fixed $\mathrm{Re}_\infty=0.06$ and $\alpha+1=16$. Given the three-dimensional parameter space and the resulting large number of simulation cases to be considered, we limited ourselves to only one spherical particle configuration per solid volume fraction. The interpretation of the thixotropic liquid results will be mainly by comparing them with corresponding results with Db=0. In doing this, we compare (per value of ϕ) simulations with the same configuration of spheres only.

A numerical issue to be dealt with when having thixotropic liquids is how to reach steady state. Since $\mathrm{Re}_\infty=0.06$ and since we have fixed $\nu_\infty=\mu_\infty/\rho=0.01$ (related to the spheres' hydrodynamic diameter calibration) the superficial velocity has to be $u_s=2.5\times10^{-5}$. We anticipate significant effects of the Deborah number on the drag force if the former is in a (broad) range around 1. In order to reach a steady flow and λ-field, simulations have to run for at least few times the liquid's time scale $1/k_2$. At Db=1, running a simulation for a time span of $1/k_2$ would imply performing 960 000 time steps. This number increases linearly with Db; the highest Db considered in this study is of the order 100. Running so many time steps for so many cases is impractical. The computational effort can be reduced drastically, however, if we realize that we are after steady-state solutions only. Then solving the scalar transport equation [Eq. (1)] can be more loosely coupled to solving the flow with the lattice-Boltzmann method.

In our time stepping approach we alternate between solving the scalar transport equation in the network parameter λ and solving the flow with the lattice-Boltzmann

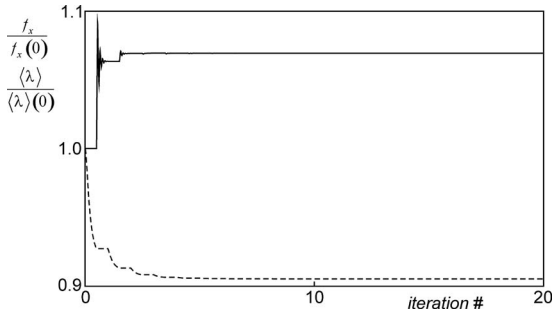

FIG. 10. Iteration history of the volume-averaged network parameter $\langle\lambda\rangle$ (dashed line) and the body force to enforce the superficial velocity f_x (solid line). Both are normalized with their initial value. Each iteration consists of 400 scalar transport steps with $\Delta t=1000$, followed by 400 LB time steps with (by definition) $\Delta t=1$.

method. We start with the steady-state solution obtained at Db=0. We freeze that flow field and solve Eq. (1) for a number of time steps, where (unlike in the lattice-Boltzmann scheme) we can take time steps much bigger than 1, usually $\Delta t=O(10^3)$. Then we freeze the scalar field and take a number of LB time steps to let the flow field adapt to the newly developed scalar field. We again freeze the flow field and again solve the scalar, etc. A typical way the system develops is given in Fig. 10, where the evolution of the volume-averaged scalar and the body force to drive the flow are given. In the portions where the force is constant only the scalar equation is solved, in the portions where the average scalar is constant only LB steps are performed. The fluctuations in the force signal are the result of a fairly stiff, however fast control algorithm used to force the superficial velocity to its desired value. For one case with a relatively small Deborah number (Db=0.2) the above iteration approach has been compared to the direct approach (solving flow and scalar transport simultaneously). The differences in the steady-state solutions (both scalar and flow) were insignificant (of the order of ten times the machine accuracy).

Examples of steady-state results are given in Fig. 11 that shows a cross section through one of the suspensions in

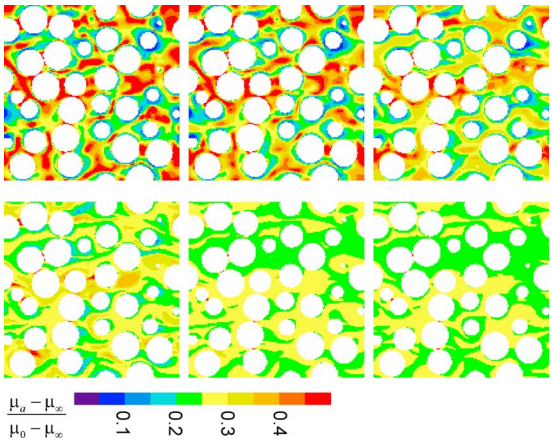

FIG. 11. (Color online) *xz*-cross sections through one flow domain, with the horizontal (x) direction the direction of the mean flow. $\phi=0.420$, $S=4$. Thixotropic simulations with (from left to right and top to bottom) Db=0, 0.2, 1.0, 5.0, 25.0, and 125.0. Shades/colors indicate the apparent viscosity.

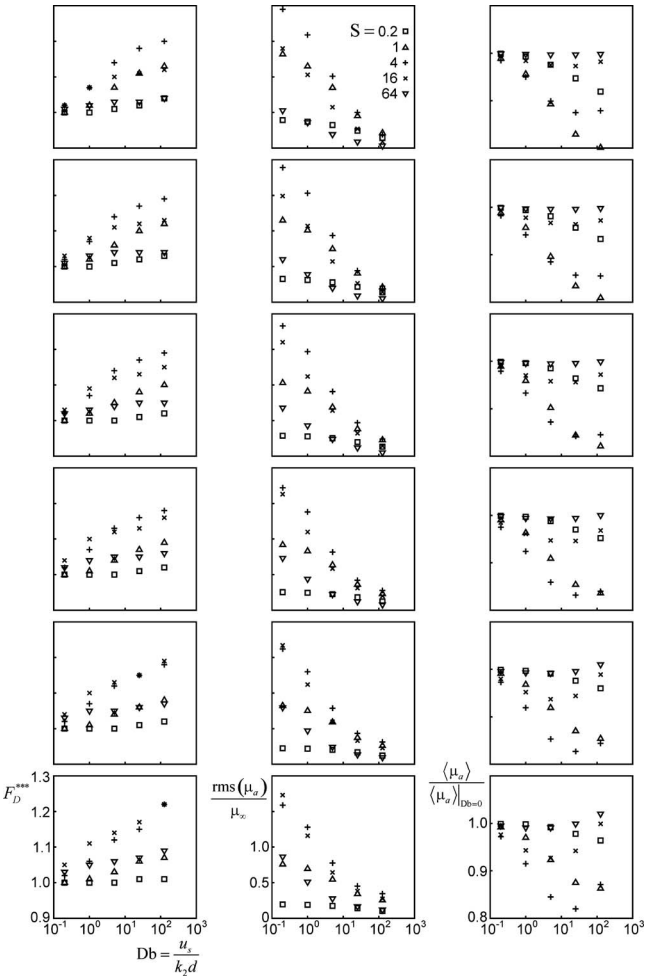

FIG. 12. Simulation results with thixotropic liquids. From left to right: triply normalized drag force, rms of viscosity, and average viscosity as a function of Db. From top to bottom: $\phi=0.330$, 0.373. 0.420, 0.459, 0.500, and 0.530. The different symbols denote different values of S as indicated.

terms of the apparent viscosity (note that the shades/color scale in Fig. 11 is different from Fig. 5). The most visible effect of thixotropy is a smearing-out of the viscosity fluctuations. This effect sets in beyond Db=0.2 (the viscosity fields at Db=0 and Db=0.2 are almost the same). The smearing-out is due to the time it takes to build up or break down the network. In an infinitely fast (Db=0) liquid, locations where the network is formed or broken down coincide with places of respectively low (e.g., bigger voids in the suspension) and high (shear layers at solid surfaces) deformation rates. If the liquid needs time to respond to deformation conditions (Db>0) the break-down and build-up processes are less localized with a smoother apparent viscosity field as the result.

In Fig. 12 the results of all of our thixotropic simulations (150 in total) are displayed, with Db as the independent variable. The triply normalized drag force is defined as $F_D^{***}\equiv F_D^{**}/F_D^{**}|_{\mathrm{Db}=0}$. The smoothing effect on the viscosity field shows as rms(μ_a) being a monotonically decreasing function of Db in all cases. The average apparent viscosity, in general slightly, reduces as a result of thixotropy (by some 20% maximum). The net effect is an increase in the drag; in

all cases considered: $F_D^{***} > 1$. The effect of thixotropy on the drag force is not very big; the maximum increase is approximately 20% (which still is significantly more than our 5% uncertainty measure related to calibration issues), occurring for high Db in situations where the corresponding Db=0 system had a large rms(μ_a).

The increased drag force, also in cases for which the *average* viscosity decreases demonstrates the relevance of the viscosity *distribution* in the suspension. In the critical regions between closely spaced sphere surfaces shear-thinning liquids reduce drag as a result of the locally high deformation rates. Thixotropy largely decouples locations of high shear with those of low viscosity thereby increasing the stresses in the critical regions, and thus increasing drag.

VI. SUMMARY

With a variety of applications in mind, the interaction of solid particles and non-Newtonian (although purely viscous) liquids has been studied. In homogeneous, steady shear the liquids would show shear-thinning behavior. In addition, the liquids are time dependent (thixotropic). By means of direct simulations, the flow of liquid between random assemblies of monosized spheres has been determined. The main interest is in the (average) drag force on a sphere, and the way it depends on the solids volume fraction, and the properties of the liquid. Only creeping flow conditions have been considered.

Solving the flow is done with the lattice-Boltzmann method on a uniform, cubic lattice. Having spherical (curved) solid-liquid interfaces in the cubic lattice requires a calibration in determining the sphere's dimension.[12,23] Since this calibration depends on the viscosity, specific care was required to control the error made this way. By choosing a high (in comparison with similar studies on Newtonian drag[6,16]) spatial resolution of $d=24$, the relative error was limited to 5%.

After it was demonstrated that Newtonian drag force results could be reproduced accurately, first time-independent, shear-thinning liquids were simulated. The strongly nonhomogeneous flow in the suspension generates an apparent viscosity field with a distribution that depends on the interplay between the flow topology (largely characterized by the solids volume fraction ϕ) and the liquid properties (most prominently its characteristic shear rate $\dot{\gamma}_c$). The viscosity distribution is widest if $\dot{\gamma}_c \approx u_s/\delta$ with δ as a measure for the typical waist size of the space in between neighboring spheres. The effect of the shear-thinning liquid properties on the drag force (scaled with its Newtonian, infinite-shear-viscosity counterpart) can be described fairly well as a unique function of the dimensionless parameter $\dot{\gamma}_c \delta/u_s$, thereby capturing the effect of the solids volume fraction.

Adding thixotropy to the physical picture can significantly change the distribution of apparent viscosities in the suspension. If the time scale of the liquid is comparable or bigger than the characteristic flow time scale (for the latter we take d/u_s), i.e., if Db$\geq$1, the gradients in the viscosity field get smoothed (in the limit of very large Db the viscosity field would get uniform). The net effect is an increase in the drag force due to an increase in the viscosity in critical (high-shear) locations in the suspension.

The results presented in this paper are clearly not universal; they specifically depend on the relatively simple rheology model [Eqs. (1) and (2)] chosen. They do show, however, interesting interactions between the flow and the apparent viscosity field, and its consequences for the drag force. They also show the role of time dependence in the liquid in a steady-state flow (dynamic properties acting on steady-state phenomena).

In future work we plan to study dynamic systems (moving spheres) to see if and to what extent non-Newtonian behavior (shear thinning, time dependence) impacts on the instabilities as, e.g., observed in fluidization/sedimentation. In this respect also the potential promotion of agglomerative behavior of particles[32] as a result of more complex liquids can be studied.

[1] J. Masliyah, Z. J. Zhou, Z. Xu, J. Czarnecki, and H. Hamza, "Understanding water-based bitumen extraction from Athabasca oil sands," Can. J. Chem. Eng. **82**, 628 (2004).
[2] B. Gueslin, L. Talini, B. Herzhaft, Y. Peysson, and C. Allain, "Flow induced by a sphere settling in an aging yield-stress fluid," Phys. Fluids **18**, 103101 (2006).
[3] A. Legrand, M. Berthou, and L. Fillaudeau, "Characterization of solid-liquid suspensions (real, large non-spherical particles in non-Newtonian carrier fluid) flowing in horizontal and vertical pipes," J. Food. Eng. **78**, 345 (2007).
[4] J. Li and J. A. M. Kuipers, "Gas-particle interactions in dense gas-fluidized beds," Chem. Eng. Sci. **58**, 711 (2003).
[5] D. Kandhai, J. J. Derksen, and H. E. A. Van den Akker, "Interphase drag coefficients in gas-solid flows," AIChE J. **49**, 1060 (2003).
[6] M. A. Van der Hoef, R. Beetstra, and J. A. M. Kuipers, "Lattice-Boltzmann simulations of low-Reynolds-number flow past mono- and bidisperse arrays of spheres: Results for the permeability and drag force," J. Fluid Mech. **528**, 233 (2005).
[7] D. Gidaspow, *Multiphase Flow and Fluidization* (Academic, Boston, 1994).
[8] B. T. Storey and E. W. Merrill, "The rheology of aqueous solution of amylose and amylopectine with reference to molecular configuration and intermolecular association," J. Polym. Sci. **33**, 361 (1958).
[9] F. Moore, "The rheology of ceramic slips and bodies," Trans. Br. Ceram. Soc. **58**, 470 (1959).
[10] T. Ferroir, H. T. Huynh, X. Chateau, and P. Coussot, "Motion of a solid object through a pasty (thixotropic) fluid," Phys. Fluids **16**, 594 (2004).
[11] A. Mujumdar, A. N. Beris, and A. B. Metzner, "Transient phenomena in thixotropic systems," J. Non-Newtonian Fluid Mech. **102**, 157 (2002).
[12] A. J. C. Ladd, "Numerical simulations of particle suspensions via a discretized Boltzmann equation. Part 2. Numerical results," J. Fluid Mech. **271**, 311 (1994).
[13] R. J. Hill, D. L. Koch, and A. J. C. Ladd, "Moderate-Reynolds-number flows in ordered and random arrays of spheres," J. Fluid Mech. **448**, 243 (2001).
[14] R. Beetstra, M. A. Van der Hoef, and J. A. M. Kuipers, "Drag force of intermediate Reynolds number flows past mono- and bidisperse arrays of spheres," AIChE J. **53**, 489 (2007).
[15] S. Benyahia, M. Syamlal, and T. J. O'Brien, "Extension of Hill–Koch–Ladd drag correlation over all ranges of Reynolds number and solid volume fraction," Powder Technol. **162**, 166 (2006).
[16] X. Yin and S. Sundaresan, "Drag law for bidisperse gas-solid suspensions containing equally sized spheres," Ind. Eng. Chem. Res. **48**, 227 (2009).
[17] J. J. Derksen and S. Sundaresan, "Direct numerical simulations of dense suspensions: Wave instabilities in liquid-fluidized beds," J. Fluid Mech. **587**, 303 (2007).
[18] S. Torquato, T. M. Truskett, and P. G. Debenedetti, "Is random close packing of spheres well defined?" Phys. Rev. Lett. **84**, 2064 (2000).
[19] S. Chen and G. D. Doolen, "Lattice-Boltzmann method for fluid flows," Annu. Rev. Fluid Mech. **30**, 329 (1998).

[20]S. Succi, *The Lattice Boltzmann Equation for Fluid Dynamics and Beyond* (Clarendon, Oxford, 2001).
[21]J. A. Somers, "Direct simulation of fluid flow with cellular automata and the lattice-Boltzmann equation," Appl. Sci. Res. **51**, 127 (1993).
[22]J. J. Derksen and Prashant, "Simulations of complex flow of thixotropic liquids," J. Non-Newtonian Fluid Mech. **160**, 65 (2009).
[23]A. Ten Cate, C. H. Nieuwstad, J. J. Derksen, and H. E. A. Van den Akker, "PIV experiments and lattice-Boltzmann simulations on a single sphere settling under gravity," Phys. Fluids **14**, 4012 (2002).
[24]A. Ten Cate, J. J. Derksen, L. M. Portela, and H. E. A. Van den Akker, "Fully resolved simulations of colliding spheres in forced isotropic turbulence," J. Fluid Mech. **519**, 233 (2004).
[25]J. J. Derksen, "Flow-induced forces in sphere doublets," J. Fluid Mech. **608**, 337 (2008).
[26]A. S. Sangani and A. Acrivos, "Slow flow through a periodic array of spheres," Int. J. Multiphase Flow **8**, 343 (1982).
[27]H. Hasimoto, "On the periodic fundamental solutions of the Stokes equations and their application to viscous flow past a cubic array of spheres," J. Fluid Mech. **5**, 317 (1959).
[28]J. J. Derksen, "Scalar mixing by granular particles," AIChE J. **54**, 1741 (2008).
[29]P. K. Sweby, "High resolution schemes using flux limiters for hyperbolic conservation laws," SIAM (Soc. Ind. Appl. Math.) J. Numer. Anal. **21**, 995 (1984).
[30]J. Derksen and H. E. A. Van den Akker, "Large-eddy simulations on the flow driven by a Rushton turbine," AIChE J. **45**, 209 (1999).
[31]J. W. Wang and W. Ge, "Collisional particle phase pressure in particle-fluid flows at high particle inertia," Phys. Fluids **17**, 128103 (2005).
[32]B. Gueslin, L. Talini, B. Herzhaft, Y. Peysson, and C. Allain, "Aggregation behavior of two spheres falling through an aging fluid," Phys. Rev. E **74**, 042501 (2006).